Applied Physics Letters

Write-once-read-many-times resistive switching behavior of amorphous barium titanate based device with very high on-off ratio and stability

Cite as: Appl. Phys. Lett. **118**, 263505 (2021); https://doi.org/10.1063/5.0050448
Submitted: 15 March 2021 . Accepted: 15 June 2021 . Published Online: 01 July 2021

Amit Kumar Shringi, Atanu Betal, Satyajit Sahu, and Mahesh Kumar

Applied Physics Letters ARTICLE scitation.org/journal/apl

Write-once-read-many-times resistive switching behavior of amorphous barium titanate based device with very high on-off ratio and stability

Cite as: Appl. Phys. Lett. **118**, 263505 (2021); doi: 10.1063/5.0050448
Submitted: 15 March 2021 · Accepted: 15 June 2021 ·
Published Online: 1 July 2021

Amit Kumar Shringi,[1] Atanu Betal,[2] Satyajit Sahu,[2] and Mahesh Kumar[1,a)]

AFFILIATIONS

[1]Department of Electrical Engineering, Indian Institute of Technology Jodhpur, Jodhpur 342037, India
[2]Department of Physics, Indian Institute of Technology Jodhpur, Jodhpur 342037, India

[a)]Author to whom correspondence should be addressed: mkumar@iitj.ac.in

ABSTRACT

Write once read many times (WORM) memory devices based on the resistive switching mechanism of a sputtered amorphous $BaTiO_3$ (am-BTO) thin film in a metal–insulator–metal structure is fabricated on a FTO coated glass substrate with a silver top contact. Fabricated devices show the switching from a low-conductance state to a high-conductance state with the formation of conductive filament(s) in the am-BTO layer. The memory characteristics are investigated as a function of thickness of am-BTO layer, which is determined by varying the deposition time. Devices with all deposited thicknesses show data retention for more than 4000 s and 300 reading cycle. Devices with 180 nm thickness show a high on-off ratio on the order of 10^6. The fabricated WORM devices exhibit good reading-endurance and data-retention characteristics.

With the rapid digitalization and widespread use of the internet of things, non-volatile memory has also received a lot of attention for its use in electronic devices and logic storage units as current Si-based electric memories are hitting its downscaling limits.[1–3] In such a scenario, resistive switching random access memory (RRAM) seems to be a good candidate for the next generation memory technology due to its low power consumption, high density integration, and fast switching operation.[4–6] Resistive switching random access memory has been studied for different types of memory characteristics such as write once read many (WORM),[7] dynamic random access memory (DRAM),[8] and flash memory.[9]

Among all types of resistive switching characteristics, WORM shows a permanent transition in its resistance state while applying a certain electric field (i.e., writing) across the device terminal. Hence, the stable memory state after writing makes it a prime choice for the applications where we need a stable and long term archival of information, images, and videos such as RF identification tags and other non-editable data devices.[10,11] With the ability of stable and permanent storage, WORM has many added advantages like low power consumption, high performance, and ease of fabrication and integration to be used as replacement of slow, expensive, and bulky mechanical drives used in conventional system for rapid and large data archival.

In recent years, variety of materials have been studied for the realization of WORM characteristics which includes organic (polymer, semiconductor, hybrid and super molecules)[12–15] and inorganic (ZnO, NiO, Al-rich Al_2O_3, HfO_2, and graphene oxide) materials.[16–20] $BaTiO_3$ thin film based resistive switching devices have been extensively studied with different substrates, deposition techniques, and temperature.[21] Metal oxide thin films are widely accepted for WORM applications due to their environmental and long term stability. In the present study, we report the WORM characteristics of RF sputtering deposited amorphous Barium titanate (BTO) deposited on FTO coated glass. The thickness of a BTO layer is varied by varying the deposition time by keeping other parameters same. Prepared samples were characterized using AFM. Simple device configuration Ag/am-BTO/FTO structures on glass are investigated as the function of thickness for WORM. For these devices, we perform the memory characterization, and we observe the low switching voltage ($\leq$1.5 V), high on-off ratio ($\approx 10^6$), long term data retention, and good reading capability.

The stoichiometric ratio of $BaCO_3$ (99.98%, Sigma Aldrich) and TiO_2 (99.8%, Sigma Aldrich) was used as a starting material and mixed thoroughly with the help of mortar and pestle in an ethanol medium. The mixed compound was annealed at 1000 °C for 5 h and

pressed into 2 in die to form a sputtering target using a hydraulic press. The prepared pellet was sintered at 1300 °C for 5 h at atmospheric conditions. We deposited the am-BTO thin film on FTO coated glass by achieving the base pressure of 7×10^{-7} mbar at room temperature. The working pressure was fixed at 2×10^{-2} mbar with 50 SCCM of Ar flow, and the applied RF power was kept at 50 W during deposition. We varied the deposition time to vary the thickness of the am-BTO thin film by 60, 90, and 120 min to achieve the thickness of 120, 180, and 240 nm, respectively. Thicknesses of deposited thin films were confirmed using a surface profilometer (Dektak XT). The prepared samples were further characterized using atomic force microscopy (AFM) to study the surface morphology.

A conventional metal insulator metal (MIM) configuration was used to fabricate devices. Silver top contacts were deposited by thermal evaporation on the am-BTO thin film using a circular shadow mask of 500 μm diameter. Ag/am-BTO/FTO devices were electrically characterized using 4200-SCS (Keithley) to analyze the WORM characteristics for −1.5–1.5 V. The low conduction state (LCS) and high conduction state (HCS) were recorded for 4000 s at 0.3 V before and after writing.

Atomic force microscopy (AFM) study has been done for all three devices to check the surface morphology using Park System (XE-70). All the images were taken in non-contact mode using NCST-Au tip with a scan speed of 0.75 lines per second and keeping the tip at a constant distance of 15 nm. The surface topography of area 10×10 nm and its line profile of devices A, B, and C are shown in Figs. 1(a)–1(c), respectively. From the figures, we can see that the surface topography of the devices is almost the same. The surface of A has an average roughness of 20.71 nm and a root mean square (rms) roughness of 26.13 nm. In contrast, B and C have average roughness of 19.91 and 20.41 and rms roughness 24.97 and 25.99 nm, respectively. Among all three devices, B has less rms roughness and also less number of small holes (black spot on the surface) on the surface. Less number of holes may decrease the leakage current for this particular device, and we will discuss it later. Line profiles on the images were drawn to take an idea on height and sizes of the clusters. All three devices show collections of a particle having a diameter of 200–750 with a maximum height of 80 nm.

The devices were electrically characterized using two probes integrated with the Keithley 4200-SCS semiconductor analyzer to check the write-once-read-many (WORM) behavior, stability, and reliability. Three devices have been made with different thicknesses of 120, 180, and 240 nm. To remember them, we named devices A, B, and C, respectively. A complete voltage iteration was applied to check the characteristics. At first, a voltage cycle of 1.5 was applied, which means applied voltage starts at −1.5 and decreases to 0, then again increases to 1.5 and comes back to 0, and goes to −1.5 V to complete the iteration. The path of applied voltage and corresponding current is shown in Fig. 2 with red arrows. With the application of −1.5 V, the devices remain at LCS, and with the decrease in negative voltage, corresponding current decreases. Figs. 2(a)–2(c) show the current-voltage characteristics of devices A, B, and C, respectively, and (d) shows the effect of stress on the performance of device B, where the absolute value of the currents in log scale is taken along the y-axis. For device A, with increasing positive voltage, current increases slowly in LCS. At a particular switching voltage of 1.09, conducting state switches to HCS and remains at a high current up to 1.5 V. while in back iteration, the current remains at the same state (HCS). Although negative voltage was applied, the conducting state does not change. Hundreds of iterations were taken, but the state was being same. The current of LCS for A was in the range of microampere. The current increases to milliampere after switching of the device, which indicates the maximum on-off ratio is 3.8×10^3 at 0.3 V. Devices B and C show similar types of behavior. For B, the LCS current is in the range of nanoampere, while increasing positive bias, the current went to the milliampere region at 1.25, which gives a very high on-off ratio of 4.6×10^6 at 0.3 V. Device C again shows LCS current in the microampere region and switches to HCS at 1.32 V applied positive bias. The maximum on-off ratio for this device is 1.2×10^3. It has been noticed that the switching voltage increases with increasing insulating oxide layer thickness of the devices although the iteration voltage for all devices remains the same, 1.5 V. In comparison of three devices, the maximum on-off ratio is highest for B, and its decreases for other two devices. 1st, 10th, 20th, and 50th iterative cycles of the devices are shown in the figure below. For B as shown in Fig. 2(d), we characterized the device for higher stress up to −4 and observed 21% degradation in reading characteristics beyond

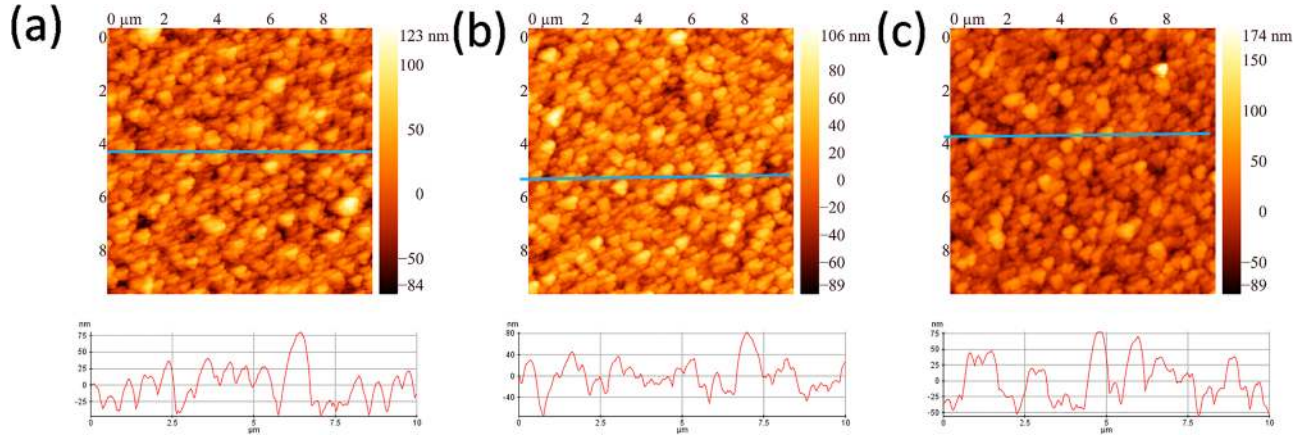

FIG. 1. Atomic force microscopy (AFM) image of area 10×10 nm was taken in non-contacting mode (NC-AFM) of the device (a) A, (b) B, and (c) C. The line profile of the surface is shown below the topography image.

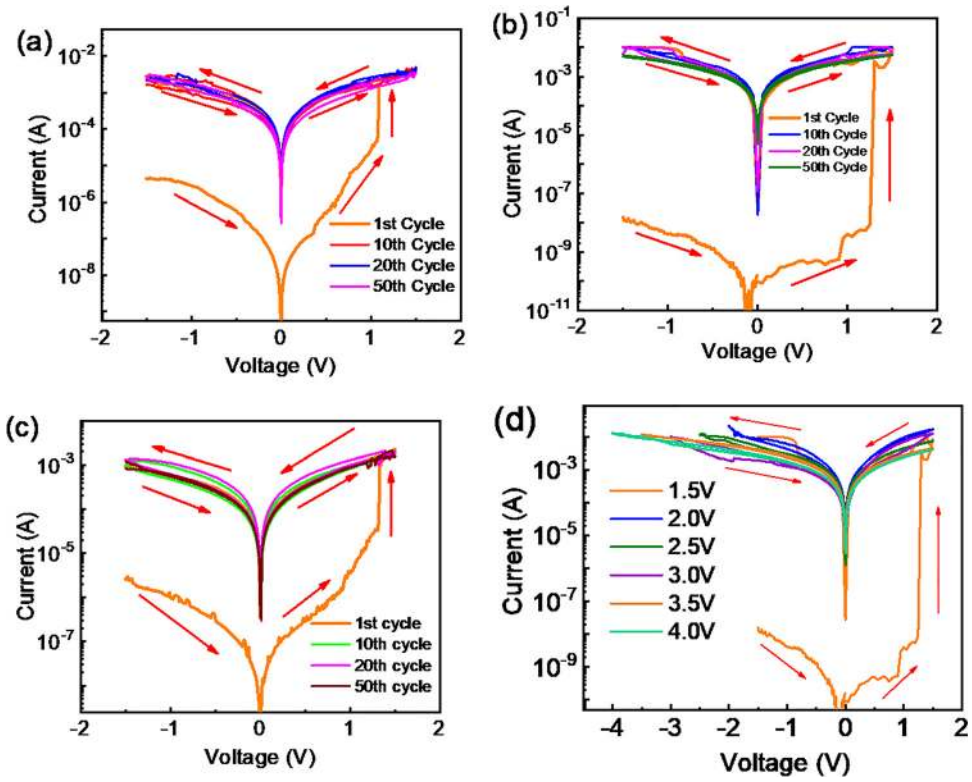

FIG. 2. Current–voltage characteristics of the devices taken at a voltage loop of −1.5–1.5 V. (a) For device A, the maximum on-off ratio is $\sim 10^3$. (b) B has a maximum ratio of $\sim 10^6$, and (c) C has $\sim 10^3$ (d) Effect of applied stress on B. The direction of applied bias and corresponding current is shown by red arrows.

−4 V as shown in the figure. The devices performed very well up to −4, but beyond −4 V, we observed degradation or filament rupturing at higher stress. Hence, we can say that the device showed stable performance up to −4 V, and beyond that, it starts degrading its programmed state. After first cycle, all other cycle remains at HCS, which means we can use these devices as highly stable and reliable resistive WORM.

The stability, reliability, and consistency of the devices have been checked by studying the data retention of the devices. The retention of A, B, and C is shown in Figs. 3(a)–3(c), respectively, and effect of reading voltage, annealing, and contact size on B is shown in Figs. 3(d)–3(f), respectively. For the WORM device, it is impossible to erase data after writing because it changes its resistive state permanently after writing the data. To check the stability, the conducting state before writing and after writing has been studied by giving a voltage pulse, and the corresponding conducting state has been noted. Four voltage pulses known as the reading pulse were given to the device per second; more than 4000 pulses were given. Before giving a write pulse, we read the current with a read voltage of 0.3 V, which was in LCS. After a voltage pulse of 1.5, named as writing voltage, the device switches to HCS. Again that particular state was checked with a read pulse of 0.3 V. For both states, it remains extremely stable as shown in the figure below.

We found that the high reading current is the common issue in almost all WORM devices including the metal fuse and poly fuse devices. Hence, we characterized the devices for low voltage reading cycle, and as we know that the reading current is a function of read voltage, we observed that there is reduction in read current at low reading voltages. Since we have a high on-off ratio on the order of 10^6, so we can easily read the devices even at lower reading voltages to reduce the overall power consumption. We have tried to reduce the reading current by applying a low reading voltage (0.1) as shown in the figure below. The reading current decreased to 1×10^{-4} for a reading voltage of 0.1 V as shown in Fig. 3(d).

Further, device B was characterized to observe the effect of annealing on post-forming state (HCS), and hence we annealed device B at 200 °C for 1 h in ambient condition after recording its HCS current. After annealing for 1 h, we characterized the device for HCS cuurent for the same reading voltage as shown in Fig. 3(e), and we observed a small reduction in HCS current. The reduction in the HCS current may be due to the migration of surface vacancies during annealing. Figure 3(f) shows the effect of contact area on the device performance. Device B was characterized for a variable contact size from 200 to 500 μm diameter deposited using a shadow mask. The device was characterized for reading current at 0.3 V for all contact sizes. We observed that with the increased contact area, the injected carriers also increased and hence result in an increased reading current. The area vs current represents electrode limited conduction rather than bulk limited conduction. Since SCLC is bulk limited conduction, it cannot be applied when we use area as a parameter to

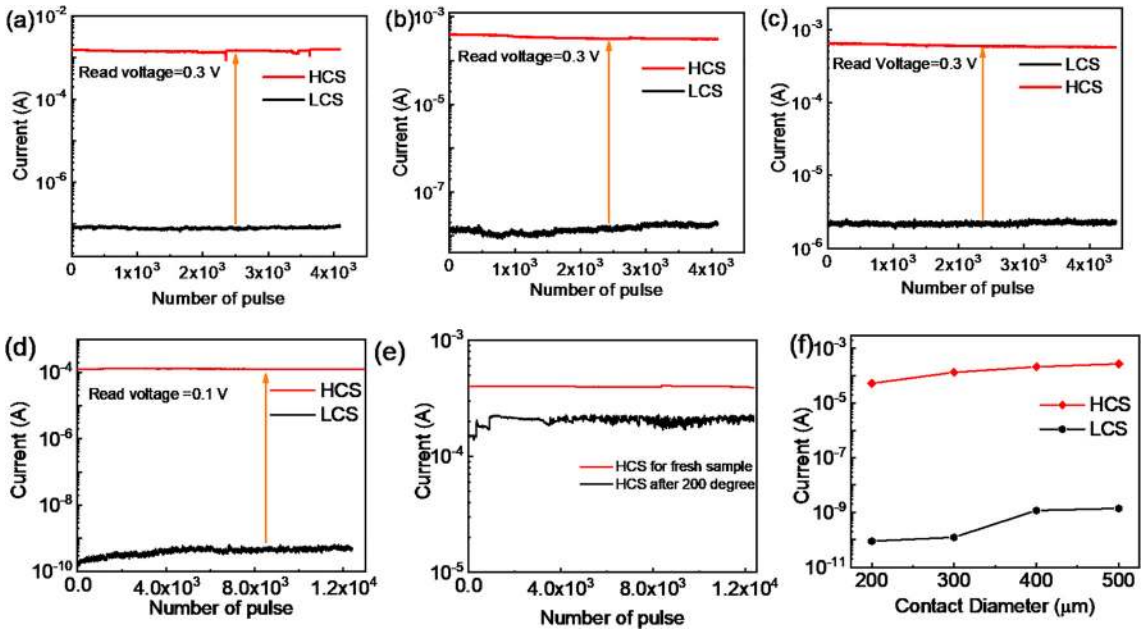

FIG. 3. (a)–(c) Data retention of devices A, B, and C, respectively. Data retention of all the devices was read at a particular read voltage of 0.3 V. (d) Reading current of device B for 0.1 V. (e) Effect of annealing on post-forming voltage for device B. (f) Effect of contact diameter on device performance.

explain its effect on conduction. Moreover, it is known that as the contact area increases, the contact resistance decreases. This provides a smaller scattering probability at the electrode dielectric interface, which helps the carriers crossover the barrier at relatively low thermal energy and get injected into the dielectric medium. Thus, the conduction mechanism which may help explain the effect is the electrode limited. Hence, as the switching mechanism is the result of the formation of conductive filaments, the area contact will influence the device resistance due to formation of conductive filament locally.

Write read erase read cycle of the devices was run to check if the written data can be accessed randomly or not and the consistency of the data even after a reverse bias was applied. The applied voltage pulse and corresponding current are shown in Figs. 4(a)–4(c) for three devices. A write, erase, and read voltage of 1.5, −1.5, and 0.3 V was taken for 4 s, 4 s, and 6 s. At first, a write voltage is applied for 4 s for the device to reach HCS and then the current is read by applying a bias of 0.3 V. Again, an erase voltage of −1.5 V was applied for 4 s to check whether the written data are erasable or not, and then the current is read at same read bias of 0.3 V. When 1.5 is applied, the devices give high current in the range of milliampere (mA), then found at high current state during reading at a bias of 0.3 V. Even after applying a reverse bias of −1.5 V, the device was found to be on the same state

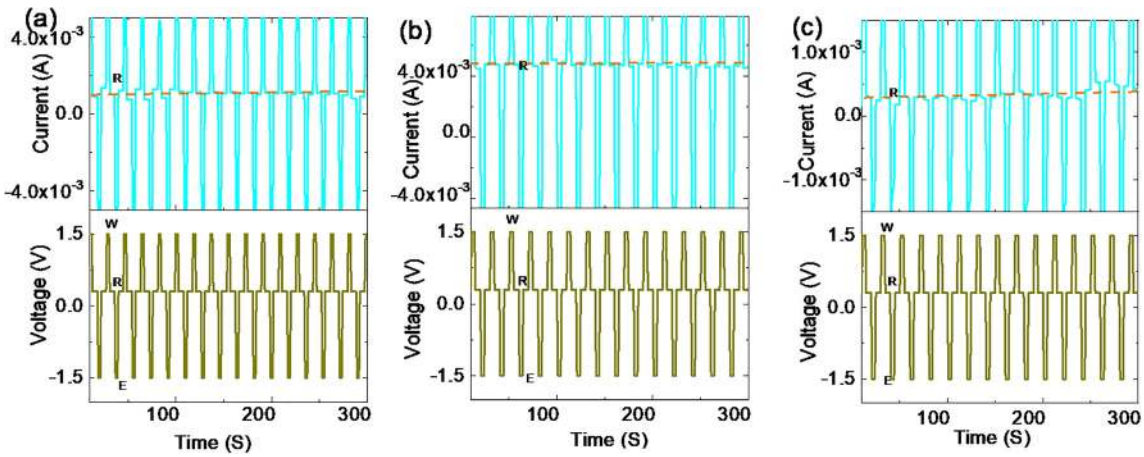

FIG. 4. Write-read-erase-read cycle of devices A, B, and C, respectively. The lower dark yellow color plots are the applied write, read, and erase voltage, while cyan color lines shows the corresponding current varying with time.

(HCS), and read current gives the same current as previous. The read current is shown with dashed lines, which shows that current is fixed before and after erase voltage. Hundreds of such cycles were taken to check its reliability, but all the devices remain extremely stable. From this, we can conclude these can be used as WORM devices.

To get an idea about the current conduction mechanism, the positive side of current voltage curves of all three devices has been plotted in logarithmic scale and fitted the data as shown in Figs. 5(a)–5(c). All the log (I)–log (V) plots show multiple slopes with COD(r^2) ≈ 0.99. Device A and C show the linear current variation with applied voltage ($I\alpha V$) and then its slope changes to more than 2 ($I\alpha V^n$, $n \geq 2$) in LCS, again showing linear variation at HCS.At the same time, B has slopes of 0.5, 2.2 in LCS and 2, 1.2 in HCS. The linear variation of current in LCS implies the direct quantum mechanical tunneling induced conduction, in which oxygen ions (vacancies) and electrons can tunnel through a potential barrier. The higher slope of log (I)–log (V) plots ($I\alpha V^n$) space charge limited conduction (SCLC). When the current varies quadratically with applied voltage ($I\alpha V^2$), it represents the trap-free SCLC for solid. The current density for SCLC is given by Mott–Gurney law,[22]

$$J = \frac{9\mu\epsilon_0\epsilon V^2}{8d^3},$$

where μ is the mobility of charge carrier, ε is the dielectric constant of the material, ε_0 is the permittivity of free space, V is the applied voltage, d is the sample thickness. The current variation ($I\alpha V^n$, $n \geq 2$) at a moderate voltage (for both HCS and LCS) is due to SCLC with trap state, which is given by

$$J_t = N_0\mu e_0^{1-l}\left(\frac{\epsilon l}{N_t(l+1)}\right)^l\left(\frac{2l+1}{l+1}\right)^{l+1}\left(\frac{V^{l+1}}{d^{2l+1}}\right),$$

where N_0 is the effective density of states in the valence band, N_t is the trap density, and l is the exponent has a value greater than one.[23] In HCS, the linear variation of current represents the Ohmic conduction where the device behaves like a metal.

The switching behavior and WORM mechanism of the fabricated device can describe by filament formation by oxygen vacancies present in the active layer. The device schematic and formation of filament are represented by Figs. 5(d)–5(f). Before applying the switching voltage, the oxygen vacancies are randomly oriented inside the active layer. When an electric field has been applied between two electrodes, some ions can move from one electrode to another, and the vacancies arranged themselves to start forming filaments. After applying sufficient bias, they form conducting filaments, and the device immediately goes to HCS. The filament forms permanently because even after giving sufficient negative pulse, it does not switch to LCS. So, it can be used as a WORM device. Furthermore, in comparison to the three devices, B shows the lowest current among them. This can be described from the AFM topography image, as said earlier. From the three images, we can see that B has fewer pinholes, which are responsible of some metallic ion penetration through the active layer. In A and C device, some metallic ions (Ag^+) penetrate through the device and

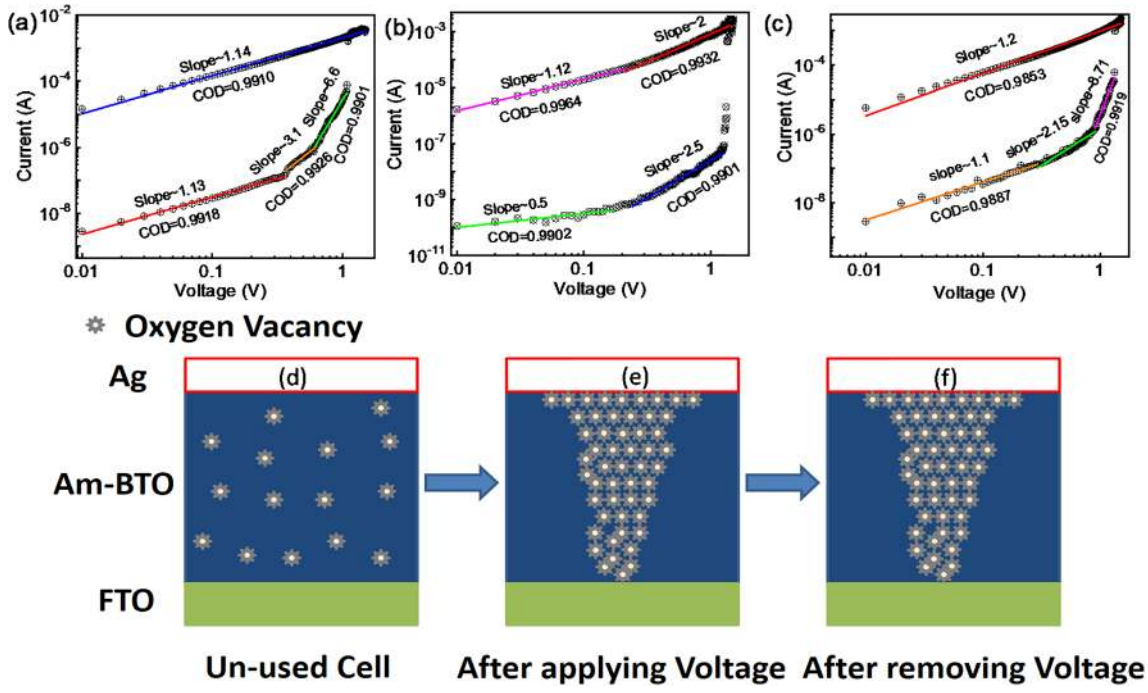

FIG. 5. (a)–(c) Current–voltage characteristics for the devices A, B, and C plotted in logarithmic scale. The plotted data were linearly fitted to get an idea of current conducting mechanism through the active layer. (d) Schematic of the devices before applying bias where oxygen vacancies are not arranged. (e) Schematic represents the formation of the filament by oxygen vacancies inside the active layer after applying switching voltage. (f) Picture showing the WORM behavior of the device in which it forms a permanent filament.

TABLE I. Comparison of recent work in the WORM area with different active materials.

Material	Deposition technique	Temperature	Switching voltage	On/off ratio	Read voltage	Read current	Speed	Reference
ZnO	RF plasma assisted MBE	400 °C	12–20 V	10^5	1 V	50 mA	···	16
IGZO	RF sputtering	RT	7 V	10^4	2 V	3 mA	1 μs	24
rGO+PVP	Spin coating	200 °C	>4 V	10^5	1 V	2 mA	700 ns	25
NiO	Pulse laser deposition	RT	3 V	10^4	0.1 V	100 mA	1 μs	17
NiO	Spin coating	550 °C	3 V	10^4	0.1 V	0.2 mA	···	26
MoS_2+ PVP	Spin coating	···	1.24 V	$>10^2$	0.1 V	1 mA	···	27
$CsPbBr_3$	Spin coating	RT	−1.1 V	10^4	0.5 V	0.1 A	···	28
$SrTiO_3$+ PVP	Spin coating	80 °C	0.17 V	$>10^3$	0.03 V	1 mA	···	4
$BaTiO_3$	RF sputtering	RT	1.5 V	10^6	0.3 V	<5 mA	105 ns	Present work

TABLE II. Comparison of existing metal fuse and poly fuse technology with current work.

Material	Deposition technique/substrate	Temperature	Programming voltage	On/off ratio	Read current	Speed	Reference
Ag-NP	Ink jet printing/ PEN	50 °C	2.6–5.5 V	$<10^8$	>1 mA	···	29
Ag-NP	Ink jet printing/paper	100 °C	3 V	10^3	>20 mA	···	30
Ag-NW	Bar coating/ PET	100 °C	2.3 V	10^6	<10 mA	<600 ms	31
PEDOT: PSS	Spin coating/ n-Si	120 °C	4 V	10^4	>10 mA	10 ms	10
PEDOT: PSS	Spin coating/ silicon	120 °C	>2 V	10^5	>100 mA	100 ms	7
$BaTiO_3$	RF sputtering/FTO	RT	1.5 V	10^6	<5 mA	105 ns	Present work

increase the current to the microampere region, while B with fewer pinholes reduces the leakage current in the nanoampere region. Furthermore, we have presented a comparison of our device performance with the work available in literature as Table I, and it can be seen that for our devices the on-off ratio is very high at a relatively low switching voltage.

Table II presents a comparative study between the existing WORM technology (metal fuse and poly fuse) with the present work in terms of their performance. We found that the present BTO devices have advantages like low switching voltage and switching speed over the compared studies.

In conclusion, Ag/am-BTO/FTO devices with different thickness were realized for WORM memory characteristics based on the resistive switching phenomenon in the MIM configuration. The devices show the switching from a low-conductance state (LCS) to a high-conductance state (HCS) by applying a low voltage signal (1.5 V). The device with 180 thickness shows the best on-off ratio on the order of 10^6 compared to 120 and 240 nm thick samples. The low on-off ratio and high current are caused by the pinholes in the surface of thin films in 120 and 240 nm samples. The fabricated devices exhibit long time date retention and good reading endurance.

DATA AVAILABILITY

The data that support the findings of this study are available from the corresponding author upon reasonable request.

REFERENCES

[1]J. J. Yang, D. B. Strukov, and D. R. Stewart, Nat. Nanotechnol. **8**, 13 (2013).
[2]B. Cho, S. Song, Y. Ji, T.-W. Kim, and T. Lee, Adv. Funct. Mater. **21**, 2806 (2011).
[3]J. Borghetti, G. S. Snider, P. J. Kuekes, J. J. Yang, D. R. Stewart, and R. S. Williams, Nature **464**, 873 (2010).
[4]G. Chen, P. Zhang, L. Pan, L. Qi, F. Yu, and C. Gao, J. Mater. Chem. C **5**, 9799 (2017).
[5]A. Sawa, Mater. Today **11**, 28 (2008).
[6]D. Ielmini, Semicond. Sci. Technol. **31**, 063002 (2016).
[7]B. C. de Brito, E. C. P. Smits, P. A. van Hal, T. C. T. Geuns, B. de Boer, C. J. M. Lasance, H. L. Gomes, and D. M. de Leeuw, Adv. Mater. **20**, 3750 (2008).
[8]Q.-D. Ling, F.-C. Chang, Y. Song, C.-X. Zhu, D.-J. Liaw, D. S.-H. Chan, E.-T. Kang, and K.-G. Neoh, J. Am. Chem. Soc. **128**, 8732 (2006).
[9]X.-D. Zhuang, Y. Chen, G. Liu, P.-P. Li, C.-X. Zhu, E.-T. Kang, K.-G. Noeh, B. Zhang, J.-H. Zhu, and Y.-X. Li, Adv. Mater. **22**, 1731 (2010).
[10]S. Smith and S. R. Forrest, Appl. Phys. Lett. **84**, 5019 (2004).
[11]S. Möller, C. Perlov, W. Jackson, C. Taussig, and S. R. Forrest, Nature **426**, 166 (2003).
[12]V. C. Nguyen and P. S. Lee, Sci. Rep. **6**, 38816 (2016).
[13]S. Shi, J. Peng, J. Lin, and D. Ma, IEEE Electron Device Lett. **30**, 1164 (2009).
[14]D. Y. Yun, J. K. Kwak, J. H. Jung, T. W. Kim, and D. I. Son, Appl. Phys. Lett. **95**, 143301 (2009).
[15]B. Mukherjee and A. J. Pal, Chem. Mater. **19**, 1382 (2007).
[16]J. Qi, Q. Zhang, J. Huang, J. Ren, M. Olmedo, and J. Liu, IEEE Electron Device Lett. **32**, 1445 (2011).
[17]Q. Yu, Y. Liu, T. P. Chen, Z. Liu, Y. F. Yu, H. W. Lei, J. Zhu, and S. Fung, IEEE Trans. Electron Devices **59**, 858 (2012).
[18]W. Zhu, T. P. Chen, Y. Liu, M. Yang, S. Zhang, W. L. Zhang, and S. Fung, IEEE Trans. Electron Devices **56**, 2060 (2009).
[19]Y. Li, X. Pan, Y. Zhang, and X. Chen, IEEE Electron Device Lett. **36**, 1149 (2015).
[20]P. C. Ooi, M. A. S. M. Haniff, M. F. M. R. Wee, C. F. Dee, B. T. Goh, M. A. Mohamed, and B. Y. Majlis, Carbon **124**, 547 (2017).

[21]P. M. Razi, S. Angappane, and R. B. Gangineni, Mater. Sci. Eng., B **263**, 114852 (2021).
[22]A. A. Grinberg, S. Luryi, M. R. Pinto, and N. L. Schryer, IEEE Trans. Electron Devices **36**, 1162 (1989).
[23]P. Mark and W. Helfrich, J. Appl. Phys. **33**, 205 (1962).
[24]P. Liu, T. P. Chen, X. D. Li, Z. Liu, J. I. Wong, Y. Liu, and K. C. Leong, Appl. Phys. Lett. **104**, 033505 (2014).
[25]M. A. Mamo, A. O. Sustaita, N. J. Coville, and I. A. Hümmelgen, Org. Electron. **14**, 175 (2013).
[26]X. L. Wang, Z. Liu, C. Wen, Y. Liu, H. Z. Wang, T. P. Chen, and H. Y. Zhang, Appl. Phys. A **124**, 454 (2018).
[27]P. Zhang, C. Gao, B. Xu, L. Qi, C. Jiang, M. Gao, and D. Xue, Small **12**, 2077 (2016).
[28]Z. Chen, Y. Zhang, Y. Yu, Y. Che, L. Jin, Y. Li, Q. Li, T. Li, H. Dai, and J. Yao, Opt. Mater. **90**, 123 (2019).
[29]R. Wang, Q. Li, L. Feng, W. Hu, W. Liu, and X. Guo, IEEE Electron Device Lett. **37**, 862 (2016).
[30]J. Leppäniemi, T. Mattila, K. Eiroma, T. Miyakawa, K. Murata, and A. Alastalo, IEEE Electron Device Lett. **35**, 354 (2014).
[31]L. Zhu, S. Chen, H. Zhou, S. Peng, Q. Zhang, X. Zhang, and X. Guo, IEEE Electron Device Lett. **39**, 347 (2018).